ACS Sustainable Chemistry & Engineering

Research Article

pubs.acs.org/journal/ascecg

Supercapacitor Electrodes Derived from Carbon Dioxide

Junshe Zhang and Jae W. Lee*

Department of Chemical and Biomolecular Engineering, Korea Advanced Institute of Science and Technology (KAIST), 291 Daehak-ro, Daejeon, 305-701, South Korea

Supporting Information

ABSTRACT: This work presents an unprecedented capacitive performance of porous carbons synthesized from carbon dioxide (CO_2). CO_2 is specifically converted to boron-doped porous carbons (BPCs) by reaction with sodium borohydride ($NaBH_4$) at 1 atm and temperatures around 500 °C. The pristine BPCs subsequently undergo treatment steps of salt removal and potassium hydroxide (KOH) activation. The activated BPCs provide specific capacitance of 130−140 F/g in a neutral solution of 1 M Na_2SO_4 after several thousand cycles. Main contributing factors to the high capacitance of the activated BPCs are their large surface area and well-defined micropores induced by the KOH activation. The observations have been elucidated by various spectroscopic and microscopic analyses.

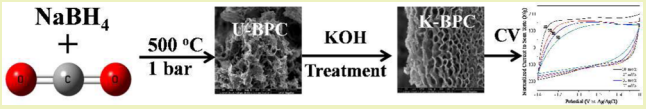

KEYWORDS: *Carbon dioxide, Boron-doped porous carbons, Supercapacitor*

INTRODUCTION

Electrochemical capacitors (ECs), also known as supercapacitors or ultracapacitors, have found a variety of applications in the area of electrochemical energy storage, ranging from portable electronics to hybrid electric vehicles and large industrial equipment, because they have high power densities, fast charge or discharge rates, and lifetimes of a million cycles.[1−3] ECs, however, have a small energy density from 2 to 5 Wh/kg, an order of magnitude lower than that of batteries,[4] which limits their widespread utilization in energy capture and storage. Thus, much effort has been made to improve their energy densities without sacrificing high power density and cycle life.[3,5−10]

The energy density of ECs (E) is proportional to the specific capacitance (C) and the square of applied voltage (V).[2] To increase the energy density, one strategy is to use organic electrolytes that can sustain high applied voltages, e.g., 2.5 to 2.7 V for electric double-layer capacitors (EDLCs, one type of ECs),[3] which store energy by using reversible ion adsorption at the electrode/electrolyte interface. Another alternative is to use carbon-based porous materials as the electrode due to their high conductivity, electrochemical stability, large surface area, moderate cost, and open porosity for EDLCs.[3] Typically, porous carbons with a specific surface area from 1000 to 2000 m^2/g and a pore size from 2 to 5 nm have a gravimetric capacitance from 100 to 200 F/g in organic electrolytes.[8]

Carbon-based electrode materials can be derived from carbon-rich organic precursors (e.g., coconut shell, petroleum coke, phenolic resin, and wood), carbides such as TiC,[11−14] graphite, or carbon nanotube.[6−10,15] Very recently, carbon dioxide (CO_2)—a readily available and sustainable carbon source—was reduced to boron-doped porous carbons (BPCs) by sodium borohydride ($NaBH_4$) at temperatures around 500 °C and atmospheric pressure.[16] Boron-doping has exhibited a great potential for enhancing the capacitance of mesoporous carbon.[17] However, BPCs derived from CO_2 have never been investigated for EDLC applications.

For carbon-based materials, a high gravimetric capacitance corresponds to a high specific surface area (SSA) and the presence of micropores (smaller than 2 nm) that contribute significantly to the capacitive storage.[3,11−13] Our results have demonstrated that the SSA of the CO_2-derived BPC is around 350 m^2/g, and it has no micropores.[16] Thus, it becomes necessary to improve the SSA of BPCs and create micropores if one wants to use them as EDLC electrodes. Potassium hydroxide (KOH) activation has been used to synthesize porous carbons with a nitrogen Brunauer−Emmett−Teller (BET) SSA of 3100 m^2/g and micropores of 1 nm from exfoliated graphite oxide.[8]

This work addresses an unexplored path to produce porous carbons with a nitrogen BET SSA of 1800 m^2/g by KOH activation of CO_2-derived BPCs and reports their unprecedented capacitive performance. The capacitive performance will be evaluated by cyclic voltammetry (CV) and galvanostatic charge/discharge at constant current densities. We will elucidate the main contributing factors to the high capacitance using numerous analyses of pristine and KOH-treated BPCs in N_2-adsorption measurements, Raman spectroscopy, scanning electron microscope (SEM), high resolution transmission electron microscope (HRTEM), elemental analyses, and X-ray photoelectron spectroscopy (XPS).

EXPERIMENTAL SECTION

Materials. Argon (Ar) with a purity of >99.9% and carbon dioxide (CO_2) with a purity of >99.8% were supplied from Deokyang Co. Ltd. Potassium hydroxide (KOH) with a purity of 99.99%, hydrochloric acid (37 wt % in water), and polytetrafluoroethylene (PTFE, 60 wt %

Received: October 10, 2013
Revised: December 13, 2013
Published: December 20, 2013

dispersion in water) were purchased from Sigma Aldrich. Sodium borohydride ($NaBH_4$) with a purity of >99% was obtained from Fluka. Sodium sulfate (Na_2SO_4) with a purity of 99.0% was supplied by Junsei Chemical. Ethanol (CH_3CH_2OH) with a purity of 99.9% was acquired from Fisher Scientific. All chemicals were used as received without further purification. Deionized (D. I.) water was produced in our lab with a resistivity of 18 MΩ cm^{-1}.

Preparation of Porous Carbon. After loading about 1.24 g of $NaBH_4$ on a 5 cm^3 alumina crucible boat (McDanel Advanced Ceramic Technologies LLC), the boat was placed into a horizontal quartz tube (Ø 25 mm) mounted inside a furnace (GSL1100X, MTI Co.). After that, the quartz tube was heated to 500 °C from room temperature in 100 min, followed by maintaining at this temperature for 2 h, and then finally cooled to room temperature under 0.1 MPa CO_2 (gauge pressure) with a flow rate of 76 cm^3 STP min^{-1}. The solid products from four repeated runs were collected and stored in a glass vial under ambient conditions. About 8.93 g of solid product was put into a 250 cm^3 glass bottle (PYREX), followed by addition of 200 cm^3 of HCl solution (5 M), resulting in a suspension of fine particles. After four days, the suspension was filtered, followed by washing the cake with D.I. water. The cake was dispersed in 200 cm^3 of D.I. water. Again, a suspension of fine particles formed, and the suspension was filtered after one day. The procedure of water-washing and then dispersing cake in 200 cm^3 D.I. water was repeated two more times. After that, the suspension was filtered, and the cake was washed with ethanol, followed by dispersing it in 200 cm^3 ethanol, which resulted in a suspension of fine particles. After the suspension was filtered, the cake was kept in the open air at room temperature for several hours and subsequently dried overnight in an oven at about 120 °C.

KOH Activation of Porous Carbon. The KOH ethanolic solution was prepared by dissolving 0.524 g of KOH in 5.64 cm^3 ethanol. About 0.15 g of porous carbon was put into a 20 cm^3 glass vial, followed by adding 2.25 cm^3 of KOH ethanolic solution. The vial was left open for several days to allow evaporation of ethanol. The sample was loaded on the alumina crucible boat, which was then put into the horizontal quartz tube mounted inside the furnace. After that, the quartz tube was heated to 100 °C from room temperature in 20 min, followed by maintaining at this temperature for 1 h. It was heated to 850 °C in 75 min, with the temperature maintained for 2 h, and then was cooled to room temperature under 0.1 MPa Ar (gauge pressure) with a flow rate of 50 cm^3 STP min^{-1}. The resultant porous carbon was put into a 20 cm^3 glass vial, followed by the addition of 20 cm^3 of HCl solution (5M), resulting in a suspension of fine particles. The suspension was placed in a closed vial for five days, after which black particulates precipitated, creating a clear supernatant. Ten cm^3 of liquid was withdrawn, to which 20 cm^3 of D.I. water was added, followed by capping the vial. A suspension formed and precipitated after one day, again resulting in a clear supernatant. The procedure of withdrawing the clear liquid and adding 20 cm^3 of D.I. water was repeated five more times, and finally 20 cm^3 ethanol was used for washing. After the clear supernatant was withdrawn in the last washing step, the resultant particles were kept in the open vial for several hours and subsequently dried overnight in an oven at ca. 120 °C.

Characterization. Elemental analyses were performed on an EA1110 CHNS-O (Thermo Finnigan) elemental analyzer to determine the composition of the bulk phase of KOH-treated porous carbon. N_2-adsorption measurements were performed at −196 °C on a Micromeritics ASAP 2020 volumetric adsorption analyzer. Before the analysis, samples were outgassed under vacuum at 200 °C for 2 h. The specific surface area, S_{BET}, was calculated by using the Brunauer−Emmett−Teller (BET) method in the relative pressure range from 0.01 to 0.06, and the total volume, V_{pore}, was estimated from the amount adsorbed at a relative pressure of 0.98. Raman spectra were obtained by using an HR800 Horiba Jobin Yvon dispersive-Raman system equipped with a CCD detector and an Olympus BX41 microscope with a ×50 objective lens. Samples were placed on a cover glass and excited with 514.5 nm Ar ion laser radiation. The spectrum was obtained by multiple spectral bandpasses between 100 and 4000 cm^{-1}. X-ray photoelectron spectroscopy (XPS) was acquired by using a MultiLab 2000 (Thermo) system equipped with Al K_α radiation ($h\nu$ = 1486.6 eV) as a probe under a chamber pressure of 5×10^{-10} mbar. The analysis spot size was 500 μm. The spectra were referenced to C 1s peak at 284.5 eV. High resolution transmission electron microscope (TEM) images were obtained with a Tecnai G2 F30 (FEI) field emission microscope operating at 300 kV. The samples for TEM were prepared by drop-casting a suspension of carbon materials in ethanol on a copper grid and then drying them under ambient conditions. Scanning electron microscope (SEM) images were obtained taken with a Magellan 400 (FEI) field emission microscope.

Electrochemical Measurements. Electrochemical measurements, including cyclic voltammetry and galvanostatic charge/discharge performed in 1 M Na_2SO_4 aqueous electrolyte at room temperature, were measured using a three-electrode configuration with Ag/AgCl as the reference electrode and Pt wire as the counter electrode. The working electrode was prepared by mixing porous carbon, carbon black, and PTFE binder with a mass ratio of 80:10:10 in water to obtain a paste, which was then dispersed on a nickel foam (current collector) as a 1 cm × 1 cm sheet before being pressed together, followed by drying at 105 °C overnight. Nickel foam was pretreated by degreasing with acetone, washing with 1 M HCl, water, and methanol sequentially, and then drying at 105 °C. Typically, the mass loading of electrode material is around 7.4 mg for the treated porous carbon and 11.5 mg for other carbon-based materials. Potential at the working electrode was controlled through a CHI 600D analyzer (CH Instrument). Before testing, the working electrode was soaked in a 1 M Na_2SO_4 aqueous electrolyte for about 3 h.

RESULTS AND DISCUSSION

The electrochemical performance of BPCs was evaluated in 1 M Na_2SO_4 aqueous electrolyte at room temperature. The cyclic voltammetry (CV) curves for untreated BPC (U-BPC) and KOH-activated BPC (K-BPC) obtained at a scan rate of 20 mV/s are shown in Figure 1. The CV curves exhibit a roughly

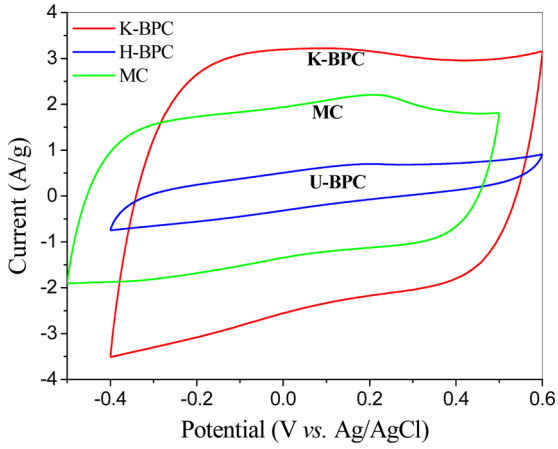

Figure 1. Cyclic voltammograms of untreated porous carbon (U-BPC), KOH-treated porous carbon (K-BPC), and ordered porous carbon (MC) in 1 M Na_2SO_4 electrolyte solution at a scan rate of 20 mV/s.

rectangular shape that is approximately symmetrical about the zero current line in a potential window from −0.4 to 0.6 V, with no obvious redox peaks corresponding to the characteristic of nearly ideal EDLCs. The area enclosed by the CV curves is proportional to the specific capacitance ($C_{s,grav}$). The enclosed areas for K-BPC and U-BPC are 4.79 and 0.68 AV/g, respectively. Thus, the KOH activation dramatically improves the electrochemical performance of BPC. For comparison, the CV curve for ordered mesoporous carbon (MC) CMK-3 (ACS MATERIALS) is also presented in Figure 1. The enclosed area for CMK-3 is 2.94 AV/g, demonstrating that the specific

dx.doi.org/10.1021/sc400414r | ACS Sustainable Chem. Eng. 2014, 2, 735−740

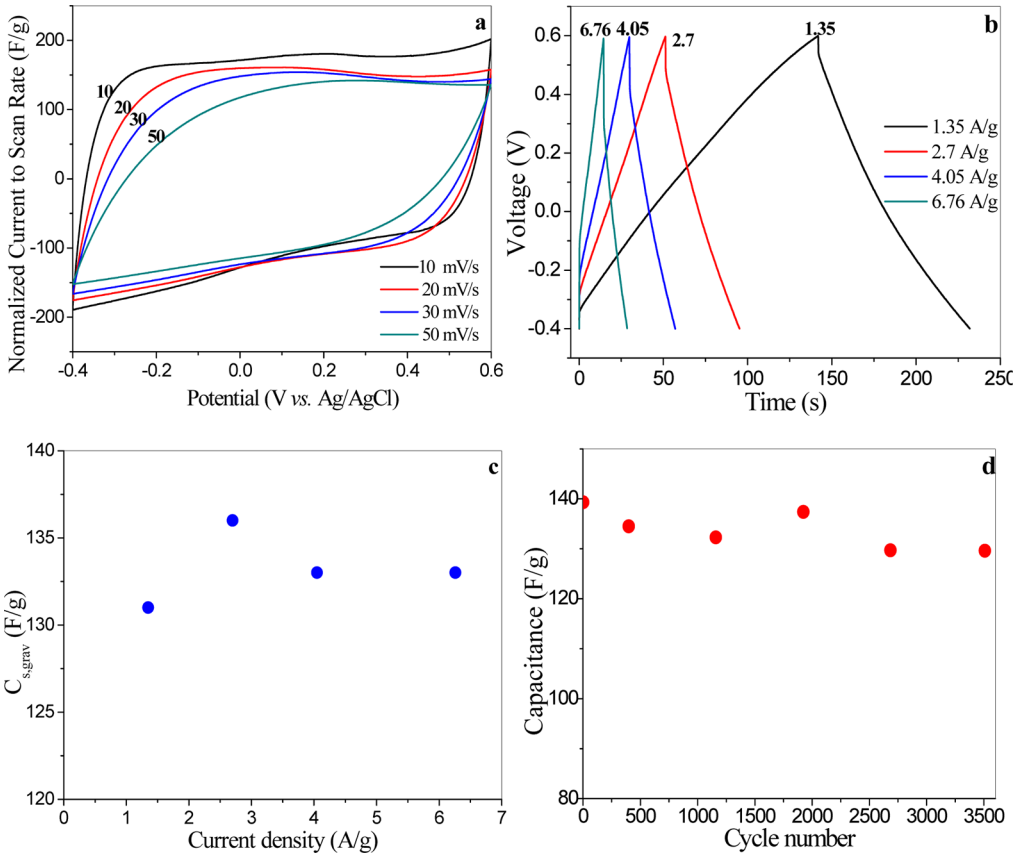

Figure 2. (a) Cyclic voltammograms of K-BPC in 1 M Na_2SO_4 electrolyte solution at 10, 20, 30, and 50 mV/s. (b) Galvanostatic charge/discharge curves of K-BPC in 1 M Na_2SO_4 electrolyte solution at 1.35, 2.7, 4.05, and 6.76 A/g. (c) Specific capacitance of K-BPC as function of discharge current density. (d) Cycle life of K-BPC at 3.3 A/g in 1.0 M Na_2SO_4 electrolyte solution.

capacitance is higher for CMK-3 than for U-BPC but is even higher for K-BPC than for the well-ordered MC (CMK-3).

The cyclic voltammograms for K-BPC at scan rates of 10, 20, 30, and 50 mV/s in the potential window from −0.4 to 0.6 V are presented in Figure 2a. As the scan rate increases, the symmetrical rectangular shape becomes distorted, along with a slight decrease in the enclosed area. This is attributed to the internal resistance of the electrical contact, electrode, and electrolyte, or the limited ion adsorption/desorption at the electrode/electrolyte interface. To obtain more information about the performance of K-BPC as electrode materials for EDLCs, we carried out galvanostatic charge/discharge measurements in the same potential window. The charge/discharge curves at constant current densities of 1.35, 2.70, 4.05, and 6.76 A/g are shown in Figure 2b. The initial portion of discharge curves exhibits an IR drop due to the internal resistance, and the rest is almost linear. In addition, the charge curves are nearly symmetrical to the corresponding discharge ones. These observations demonstrate that the capacitance of K-BPC originates from the ion adsorption/desorption at the electrode/electrolyte interface.

Moreover, a close examination of Figure 2b reveals that the initial IR drop for the current density of 1.35 A/g is 0.065 V. According to the method proposed by Stoller and Ruoff,[18] the internal resistance calculated from the IR drop and total current change is found be 3.25 Ω, close to that for U-BPC (data not shown here). Thus, we believe that the KOH activation has little effect on the resistance of BPC.

Galvanostatic discharge data are employed to calculate the specific capacitance, $C_{s,grav}$,[18] according to $C_{s,grav}(F/g) = I \times \Delta t/\Delta E$ from the discharge curve, where I is the discharge current density (A/g), Δt is the discharge time (s), and ΔE is the potential window during discharge process after the IR drop. Figure 2c shows the specific capacitance at different discharge current densities. Interestingly, the specific capacitance maintains around 133 F/g as the discharge current density increases from 1.35 to 6.76 A/g. The same behavior showing the constant specific capacitance regardless of the current densities is also observed for other carbon-based supercapacitors.[5,8] In addition, the specific capacitance of K-BPC is higher than that of other ordered mesoporous carbons. For example, $C_{s,grav}$ for undoped and heteroatom-doped mesoporous carbons in 1.0 M H_2SO_4 aqueous electrolyte is lower than 120 F/g.[17] Usually, the carbon-based materials have a lower capacitance in Na_2SO_4 than in the H_2SO_4 electrolyte.[19] Therefore, K-BPC exhibits better electrochemical performance than the ordered mesoporous carbons.[17]

Because a long cycle life is crucial for supercapacitor operations, the cycling stability was tested by using galvanostatic charge/discharge cycles at 3.3 A/g. As shown in Figure 2d, the specific capacitance of the first cycle is 139 F/g, and it decreases to 130 F/g after 3510 cycles. Thus, K-BPC also has a good cycling performance because it retains 93% of the initial capacitance even subject to repeated use.

To gain more insight into the high electrochemical performance of K-BPC, we characterized it by using high resolution nitrogen adsorption at 77.3 K, Raman spectroscopy,

dx.doi.org/10.1021/sc400414r | ACS Sustainable Chem. Eng. 2014, 2, 735−740

scanning electron microscopy (SEM), high-resolution transmission electron microscopy (HRTEM), and X-ray photoelectron spectroscopy (XPS). As shown in Figure 3a, K-BPC

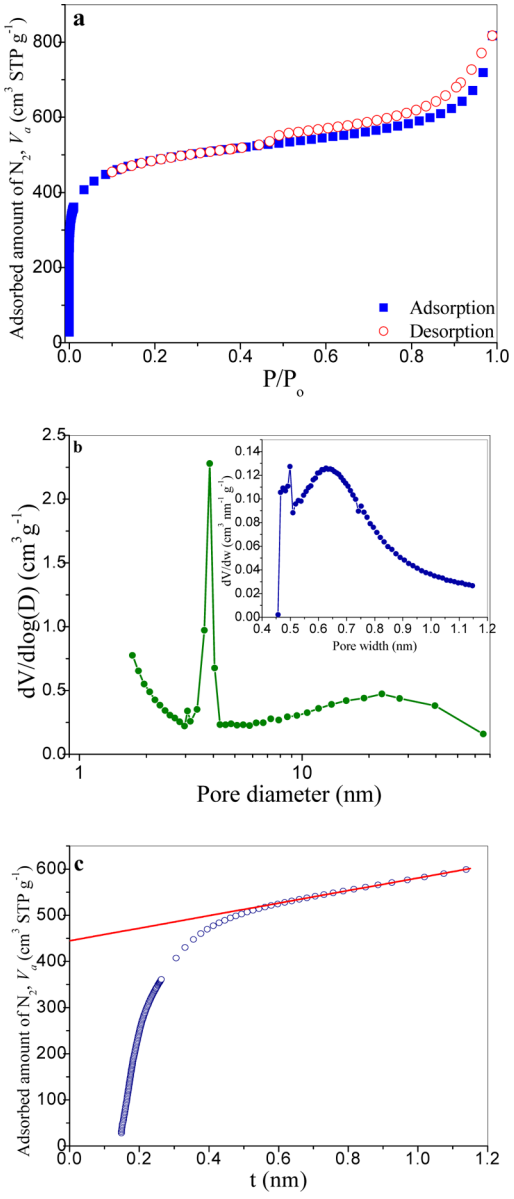

Figure 3. (a) N_2 adsorption−desorption isotherms on K-BPC at 77.3 K. (b) Pore size distribution. (c) *t*-Plot of adsorption isotherm.

gives a composite adsorption isotherm without a distinctive plateau, with the initial section being a type I isotherm but the high-pressure region exhibiting a type II isotherm along with a type H3 hysteresis.[20] These observations reveal that K-BPC contains pores with a wide range of sizes cross the micropore−mesopore boundary. The micropore size (<2 nm) distribution was determined by using the Horvath−Kawazone (HK) method, whereas the mesoporous size (2−50 nm) distribution was estimated by means of Barrett−Joyner−Halender (BJH) methods, and the results are illustrated in Figure 3b. The pore volume distribution curve exhibits a principal peak at 0.63 nm at a pore size range from 0.45 to 1.14 nm, but it has one sharp peak at 3.8 nm and another broad peak at 22.8 nm at a pore size range from 1.74 to 65.2 nm. These results suggest that the KOH activation produces well-defined micropores because such a characteristic is absent for U-BPC.[16]

This microstructural difference, however, cannot be inferred from SEM images, as shown in Figure 4a and b. These images reveal that porous carbon was partially etched during KOH activation, which is responsible for the generation of micropores. The BET SSA, calculated from the relative pressure range from 0.01 to 0.06, is ~1800 m^2/g, which is about 5 times as high as that for U-BPC.[16] The total pore volume is 1.2 cm^3/g, and the volume of micropores, estimated from the *t*-plot (*t* stands for statistical thickness in Figure 3c), is 0.7 cm^3/g. The external surface area (calculated from the *t*-plot) is ~200 m^2/g, which is due to very small particles. The high BET SSA, together with the presence of micropores, accounts for the enhanced specific capacitance.

Raman spectroscopy is an effective and nondestructive tool to characterize the disorder structure of graphitic materials.[21] Raman spectra for U- and K-BPC (Figure 5) exhibit two most pronounced peaks; they are the *D* band at about 1358 cm^{-1} and *G* band at about 1590 cm^{-1}. In addition, a weak and broadened band is observed between 2250 and 3350 cm^{-1}, which is attributable to a combination of 2D, D + G, and 2G modes. A further analysis of Raman spectra reveals that the intensity ratio of the *D* to *G* band becomes higher after the KOH activation as shown in Figure 5, indicating a decrease in microstructure ordering. Our previous results demonstrate that U-BPC is amorphous, thus K-BPC is expected to be a noncrystalline graphitic material. As shown in Figure 4c and d, HRTEM images exhibit that no well-ordered structure can be identified in K-BPC.

Boron, or other elements, was found to enhance the electrochemical performance of porous carbons by generating pseudocapacitance and modifying the electronic structure.[17] Compositional information about the surface of carbon-based materials can be obtained from XPS analysis. For U-BPC, the XPS B1s spectrum displays two principal peaks at about 188 and 191 eV (Figures S1 and S2, Supporting Information), corresponding to B−C (B_4C) and O−B−C (BCO_2) species of the carbon network into which boron atoms are incorporated, respectively.[16,22,23] For K-BPC, only C and O are detected (Figure S3, Supporting Information). However, the incorporation of B into the carbon network could not be excluded because XPS only provides the composition of the outermost layer, with a penetration depth from 5 to 15 nm.[24,25] Also, the bulk atom fraction of B for K-BPC is estimated to be about 0.034 from elemental analyses. Nevertheless, it appears that B-doping may not significantly contribute to the enhanced capacitance.

CONCLUSIONS

We have demonstrated that boron-doped porous carbons (BPCs) were produced from carbon dioxide at mild conditions and that the KOH activation of BPCs provided good electrochemical performance, which makes BPCs useful as electrode material for supercapacitors. Also, our observations have shown that chemical activation dramatically enhances the surface area of BPCs, along with generation of their micropores. Because pore size has a significant effect on electrical double-layer capacitance, our current efforts focus on designing CO_2-derived porous carbons with a large volume of narrow but small pores to improve both energy and power density.

dx.doi.org/10.1021/sc400414r | ACS Sustainable Chem. Eng. 2014, 2, 735−740

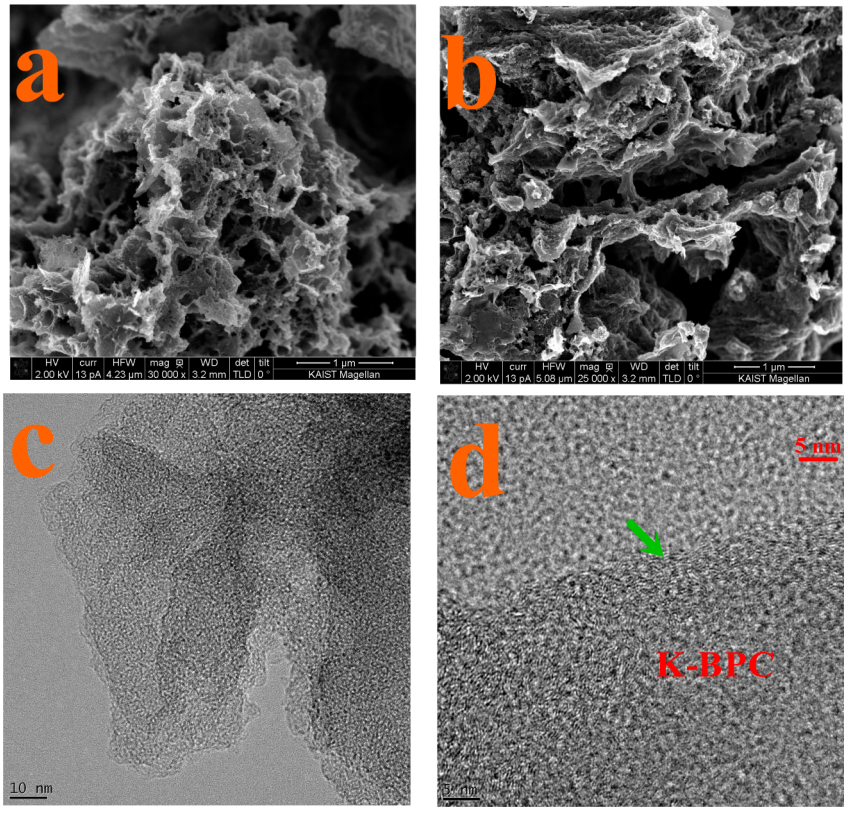

Figure 4. Representative SEM images of U-BPC (a), K-BPC (b), and HRTEM images of K-BPC (c, d). The arrow in (d) points the boundary between grid and K-BPC sample; the lower part is K-BPC.

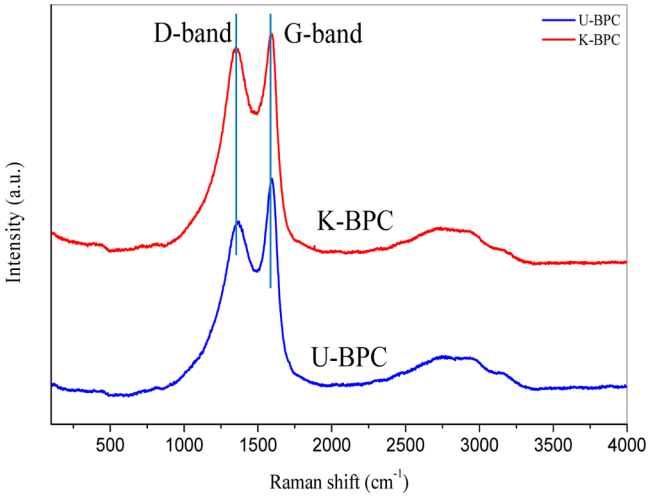

Figure 5. Raman spectra of U-BPC and K-BPC.

■ ASSOCIATED CONTENT

Supporting Information

XPS spectra of pristine BPCs and KOH-treated BPCs. This material is available free of charge via the Internet at http://pubs.acs.org.

■ AUTHOR INFORMATION

Corresponding Author

*E-mail: jaewlee@kaist.ac.kr. Tel: 82-42-350-3940. Fax: 82-42-350-3910.

Funding

The authors are grateful for the financial support from the Korea CCS R&D Center funded by the Ministry of Science, ICT, and Future Planning (NRF-2013M1A8A1040703).

Notes

The authors declare no competing financial interest.

■ REFERENCES

(1) Conway, B. E. *Electrochemical Supercapacitors: Scientific Fundamentals and Technical Applications*; Kluwer Academic/Plenum: New York, 1999.
(2) Simon, P.; Gogotsi, Y. Materials for electrochemical capacitors. *Nat. Mater.* **2008**, *7*, 845−854.
(3) Miller, J. R.; Simon, P. Electrochemical capacitors for energy management. *Science* **2008**, *321*, 651−652.
(4) Abruña, H. D.; Kiya, Y.; Henderson, J. C. Batteries and electrochemical capacitors. *Phys. Today* **2008**, *61*, 43−47.
(5) Stoller, M. D.; Park, S.; Wu, Y.; An, J.; Ruoff, R. S. Graphene-based ultracapacitors. *Nano Lett.* **2008**, *8*, 3498−3502.
(6) Lv, W.; Tang, D. M.; He, Y. B.; You, C. H.; Shi, Z. Q.; Chen, X. C.; Chen, C. M.; Hou, P. X.; Liu, C.; Yang, Q. H. Low-temperature exfoliated graphenes: Vacuum-promoted exfoliation and electrochemical energy storage. *ACS Nano* **2009**, *3*, 3730−3736.
(7) Miller, J. R.; Outlaw, R. A.; Holloway, B. C. Graphene double-layer capacitors with AC line-filtering performance. *Science* **2010**, *329*, 1637−1639.
(8) Zhu, Y.; Murali, S.; Stoller, M. D.; Ganesh, K. J.; Cai, W.; Ferreira, P. J.; Pirkle, A.; Wallace, R. M.; Cychoze, K. A.; Thommes, M.; Su, S.; Stach, E. A.; Ruoff, R. S. Carbon-based supercapacitors produced by activation of graphene. *Science* **2011**, *332*, 1537−1541.
(9) El-Kady, M. F.; Strong, V.; Dubin, S.; Kaner, R. B. Laser scribing of high-performance and flexible graphene-based electrochemical capacitors. *Science* **2012**, *335*, 1326−1330.

(10) Chen, J.; Li, C.; Shi, G. Graphene materials for electrochemical capacitors. *J. Phys. Chem. Lett.* **2013**, *4*, 1244−1253.
(11) Chmiola, J.; Yushin, G.; Gogotsi, Y.; Portet, C.; Simon, P.; Taberna, P. L. Anomalous increase in carbon capacitance at pore sizes less than 1 nanometer. *Science* **2006**, *313*, 1760−1763.
(12) Chmiola, J.; Largeot, C.; Taberna, P. L.; Simon, P.; Gogotsi, Y. Desolvation of ions in subnanometer pores and its effect on capacitance and double-layer theory. *Agnew. Chem., Int. Ed.* **2008**, *47*, 3392−3395.
(13) Largeot, C.; Portet, C.; Chmiola, J.; Taberna, P. L.; Gogotsi, Y.; Simon, P. Relation between the ion size and pore size for an electric double-layer capacitor. *J. Am. Chem. Soc.* **2008**, *130*, 2730−2731.
(14) Chmiola, J.; Largeot, C.; Taberna, P. L.; Simon, P.; Gogotsi, Y. Monolithic carbide-derived carbon films for micro-supercapacitors. *Science* **2010**, *328*, 480−483.
(15) Lu, W.; Hartman, R.; Qu, L.; Dai, L. Nanocomposites electrodes for high-performance supercapacitors. *J. Phys. Chem. Lett.* **2011**, *2*, 655−660.
(16) Zhang, J. S.; Lee, J. W. Production of boron-doped porous carbon by the reaction of carbon dioxide with sodium borohydride at atmospheric pressure. *Carbon* **2013**, *53*, 216−221.
(17) Wang, D. W.; Li, F.; Chen, Z. G.; Lu, G. Q.; Cheng, H. M. Synthesis and electrochemical property of boron-doped mesoporous carbon in supercapacitor. *Chem. Mater.* **2008**, *22*, 7195−7200.
(18) Stoller, M. D.; Ruoff, R. S. Best practice methods for determining an electrode material's performance for ultracapacitors. *Energy Environ. Sci.* **2010**, *3*, 1394−1301.
(19) Kim, H.; Povo, B. V. Synthesis and characterization of MnO_2-based mixed oxides as supercapacitors. *J. Electrochem. Soc.* **2003**, *150*, D56−62.
(20) Rouquerol, F.; Rouguerol, J.; Sing, K. *Adsorption by Powders and Porous Solis: Principles Methodology and Application*; Academic Press, London, 1999.
(21) Ferrari, A. C.; Robertson, J. Interpretation of raman spectra of disordered and amorphous carbon. *Phys. Rev. B* **2000**, *61*, 14095−14107.
(22) Yang, L.; Jiang, S.; Zhao, Y.; Zhu, L.; Chen, S.; Wang, X.; Wang, Q.; Ma, J.; Ma, Y.; Hu, Z. Boron-doped carbon nanotubes as metal-free electrocatalysts for the oxygen reduction reaction. *Angew. Chem., Int. Ed.* **2011**, *50*, 7132−7135.
(23) Wu, Z.; Ren, W.; Xu, L.; Li, F.; Cheng, H. Doped graphene sheets as anode materials with superhigh rate and large capacity for lithium ion batteries. *ACS Nano* **2011**, *5*, 5463−5471.
(24) Figueiredo, J. L.; Pereira, M. F. R.; Freitas, M. M. A.; Orfao, J. J. M. Modification of the surface chemistry of activated carbons. *Carbon* **1999**, *37*, 1379−1389.
(25) Darmstadt, H.; Roy, C.; Kaliaguine, S.; Choi, S. J.; Ryoo, R. Surface chemistry of ordered mesoporous carbons. *Carbon* **2002**, *40*, 2673−2683.